Enhancing thermoelectric properties of $NaCo_2O_4$ ceramics through Na pre-treatment induced nano-decoration

E.M. Jakubczyk [a], A. Mapp [a], C.C. Chung [b], C.L. Sansom [c], J.L. Jones [b], R.A. Dorey [a, *]

[a] Centre for Engineering Materials, Mechanical Engineering Sciences, University of Surrey, Surrey, Guildford, Surrey, GU2 7XH, UK
[b] North Carolina State University, Materials Science and Engineering, Raleigh, NC, USA
[c] Cranfield University, Cranfield, Bedfordshire, MK43 0AL, UK

ABSTRACT

High quality $NaCo_2O_4$ thermoelectrics are challenging to process due to the volatile nature of Na, the slow densification kinetics, and degradation of $NaCo_2O_4$ above 900–950 °C leading to the formation of Na-poor second phases. Fine grained sol-gel derived powders have been used to enhance the densification kinetics while pre-treatment of the $NaCo_2O_4$ powder with NaOH, to provide a Na rich environment, has been shown to mitigate Na loss at elevated temperatures. While insufficient to compensate for Na loss at processing temperatures of 1000 °C and above, at lower temperatures it is able to enhance densification and facilitate the formation of complex crystal structures yielding low thermal conductivity (0.66 $Wm^{-1}K^{-1}$) coupled with high electrical conductivity (3.8×10^3 Sm^{-1}) and a Seebeck coefficient of 34.9. The resultant room temperature power factor and ZT were 6.19×10^{-6} $Wm^{-1}K^{-2}$ and 0.0026, respectively.

© 2019 Published by Elsevier B.V.

1. Introduction

Thermoelectric (TE) materials have the potential to play a significant role in the development of sustainable energy-efficiency technologies due to their ability to directly convert heat into electricity with no moving parts [1]. The relative performance of thermoelectric materials can be described by the dimensionless figure of merit [2,3], $ZT = S^2\sigma T/\kappa$, where T is temperature. High efficiency thermoelectric power generation thus requires low thermal conductivity (κ) and at the same time, a high Seebeck coefficient (S) and electrical conductivity (σ) [4]. ZT should ideally be > 1 to achieve conversion efficiencies greater than 10% [1]. As such there is a significant drive to increase ZT, particularly at high temperatures. At elevated temperatures traditional TE materials, such as Bi_2Te_3, are known to melt and oxidize in the presence of air [5,6]. Furthermore such materials are composed of toxic, heavy and rare elements leading to active research into replacement materials such as oxide ceramics [5]. There are a number of candidate materials including $NaCo_2O_4$, $Ca_3Co_4O_9$ and modified $SrTiO_3$ that have been shown to exhibit useful properties, however they contain volatile elements and necessitate high processing temperatures, typical of ceramics, which can lead to loss of stoichiometry and grain growth which are detrimental for thermoelectric properties.

Thermal and electrical conductivities are linked as both rely on conduction of electrons. However thermal conductivity is also dependent on the transmission of phonons. As such it is possible to decouple the two conductivities by disrupting phonon conduction leading to an improvement in TE performance [7]. The thermal conductivity of polycrystalline ceramics, such as sodium cobalt oxides, is strongly correlated with the crystal structure [8], as well as particle morphology and microstructural defects. $NaCo_2O_4$ has a layered hexagonal crystal structure consisting of CoO_2 layers separated by Na ions. Electrical conductivity is achieved in the CoO_2 nanosheets by the donation of electrons from Na. The Na ion nano-layers serve as phonon scattering structures [9]. The crystal structure gives rise to anisotropy in electric and thermal properties with higher conductivity exhibited parallel to the CoO_2 planes which in polycrystalline ceramics leads to a decrease in phonon conduction [10]. $NaCo_2O_4$ thermal conduction is dominated by phonons [9,10] and hence significant improvements in thermoelectric performance can be achieved by disrupting this transport.

By creating scattering points on the length scale of a few 10s of nm electron conduction is unaffected while phonon conduction is dramatically reduced due to their different characteristic mean free paths. Small grain size can enhance the specific grain boundary

(GB) surface area with a reduction in thermal conductivity due to grain boundary scattering of phonons [11]. Thermal conductivity can also be reduced by modification of the nanostructure of these materials [12]. Nanostructured materials exhibit unique properties including enhanced density of states (DOS) near Fermi level via quantum confinement and a large density of interfaces [13,14] which are not observed in bulk materials. Such structures, and the resultant properties, are strongly dependent on the material preparation method.

Sodium cobalt oxide is a promising functional ceramic material for TE applications, however, working with high-volatility elements such as sodium presents challenges in maintaining a stable material composition throughout processing. Nano-sized powders can increase sintering kinetics and allow materials to be processed at lower temperatures, helping to reduce Na volatisation and stabilise the material composition. Methods for the production of nano-sized sodium cobalt oxide have been reported based on electrospinning of nanofibres [15,16] from sol-gel materials to produce nanofibres about 10 nm in diameter, an order of magnitude smaller than sodium cobalt oxide powders produced by conventional methods. The sol-gel method is one of the most effective production methods for fine powders [17]. The processing conditions for these materials can influence both the sodium content and the development of the cobalt oxide layer structure due to the presence of mixed-valence Co as well as different relative positions of the CoO_2 layers, depending on sodium content. Even when starting from nanoscale powders it is imperative that grain growth is controlled to prevent increases in thermal conductivity. Here we consider the use of sol-gel derived material to attain fine sinterable powders suitable for low temperature processing with limited grain growth. To enhance low temperature densification and alleviate the issue of Na loss at elevated temperatures the use of a Na-rich pre-treatment of the powder is also explored.

2. Material and methods

A $NaCo_2O_4$ powder was synthesised using an aqueous sol-gel method and used to produce bulk pellets. 0.11 mol of $Co(NO_3)_2 \cdot 6H_2O$, 0.094 mol $NaNO_3$ and 0.13 mol $C_6H_8O_7$ were dissolved in distilled water to obtain a 0.3 M solution. The solution was stirred constantly at 80 °C for 1.5 h to achieve a homogenous solution. The resulting mixture was light red in colour and was allowed to cool while being stirred. The prepared $NaCo_2O_4$-producing sol was dried in an oven at 90 °C to produce a light pink precursor powder.

The dried precursor powder was crushed and heated to 700 °C at a ramp rate of 4 °C/min to calcine the powder for 6 h. A modified powder (Na-SG) was created by ball milling the calcined powder for 24 h in a sodium hydroxide aqueous solution (2 wt% NaOH relative to $NaCo_2O_4$ powder mass). Suspensions were milled using weight ratios of 1:2:1 of powder:ZrO_2 milling media:fluid. To prevent Si contamination during the ball milling stage of preparation, plastic bottles were used. The resulting slurry was dried overnight in an oven at 70 °C.

Pellets were created from both powders by crushing with a mortar and pestle and pressing in a 3 cm diameter mould at 1.3 MPa. The pellets were sintered at 950 °C or 1000 °C for 1, 2, 6 or 12 h at a heating ramp rate of 4 °C/min a furnace cooling. The pellets referred to as SG were made from pure sol-gel powder and Na-SG pellets were made from sol-gel powder that had previously been ball milled in an aqueous solution of NaOH.

All sintered samples were examined by X-ray diffraction (XRD) (Siemens 5005) at room temperature. The microstructures of the as-sintered samples were examined using a scanning electron microscope (FEI XL30 SFEG) and energy dispersive X-ray spectroscopy (EDX). Density was determined from the measured weight and dimensions of the pellets. Phase formation and phase transition behaviours of the powder were investigated using a Panalytical Empyrean X-ray diffractometer with an Anton Parr HTK 1200 N high temperature oven chamber. Dried and crushed as-synthesised powder was initially heated up to 200 °C for 15 min to reduce organic components. The sample was then placed in the XRD chamber and heated from 25 °C to 1000 °C with a heating rate of 5 °C/min. Diffraction patterns were measured throughout the whole heat treatment using Cu Kα x-ray radiation with a wavelength of 1.5418 Å and a 2θ range of $30° - 45°$. Each pattern was measured for 4 min using a step size and count time of 0.0263° 2θ and 39 s/step, respectively. Both dried precursor powder and dried precursor powder modified with NaOH were examined.

Thermal conductivity of samples was measured using a comparative bar method employing glass standards of known thermal conductivity. The sample was sandwiched between two known standards with thermocouples positioned either side of each sample. By assuming the heat flux was the same through all samples the thermal conductivity of the test sample could be calculated. Electrical conductivity was determined by 4 point probe method and Seebeck coefficient by measuring the voltage generated by the sample following the application of a known temperature difference across it.

3. Results and discussion

3.1. Sintering and microstructure

Figs. 1(a) and 2(a) shows a contour plot of in situ XRD patterns illustrating the evolution of the SG powder and Na-SG powder, respectively. At lower temperatures the peaks associated with Co_3O_4 (having formed following the decomposition of $Co(NO_3)_2 \cdot 6H_2O$ during initial preheating) are clearly visible and gradually shift to lower angles due to thermal expansion (e.g. (311) peak between 36.5 and 37.0° shown in Figure (b)). In both powder systems there is a clear indication of a phase change occurring at around 650 °C to produce the desired $NaCo_2O_4$. Initially the peaks associated with Co_3O_4 decrease in intensity and eventual disappear as $NaCo_2O_4$ is produced on reaction with Na. In the case of the SG powder there is also evidence of the formation of a $Na_{0.6}Co_2O_4$ phase as an intermediate product. This is not evident in the Na-SG powders showing that excess Na aids in the formation of phase pure material. $NaCo_2O_4$ is stable up to around 900 °C when it degrades from this optimum composition over a temperature range around 900–950 °C. At temperatures exceeding 950 °C new peaks appear indicating the formation of CoO as a consequence of the reduction of residual Co_3O_4 and Co_3O_4 formed as Na is lost from $NaCo_2O_4$. Interestingly the Na-SG powder appears less stable despite having more Na present suggesting that Na removal from the crystal lattice may be enhanced by the presence of a small amount of liquid NaOH at the surface of the powder. The loss of Na can be seen quantitatively when comparing solid state synthesis material, sol gel material and Na-sol gel materials sintered at 1000 °C for 6 h, where Na:Co atomic ratios of 0.24, 0.40 and 0.55 (± 0.1) are observed, respectively. Fine grained starting material (i.e. SG) leads to more rapid densification and hence reduced Na loss, while addition of 10 at% extra Na helps to further stabilise the system.

This formation temperature of $NaCo_2O_4$ (650 °C) is significantly lower than that for conventional solid state reaction produced material, where the correct $NaCo_2O_4$ composition is only obtained at around 750–850 °C [18]. The sol-gel approach therefore represents a potentially lower temperature and more cost-effective processing route for the $NaCo_2O_4$ based materials. In the case of Na-SG material in-situ X-ray diffraction also revealed that
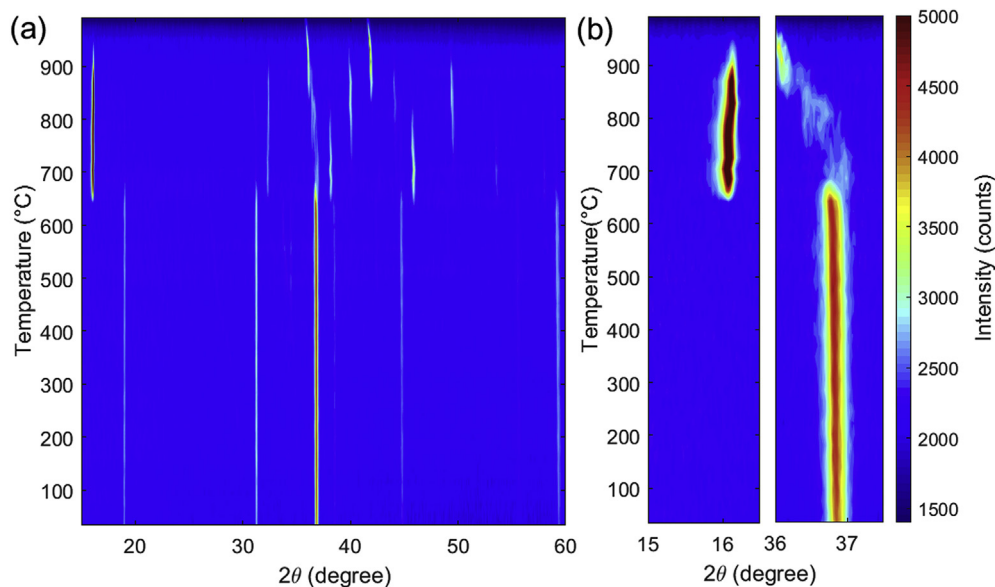
Fig. 1. In situ XRD patterns of dried precursor sol gel powder collected at various temperatures from room temperature up to 1000 °C, (a) contour plot of in situ XRD patterns, (b) 2θ region of 15–16.5° and 36–37.5° showing the evolution of most intense peak corresponding to reaction during sol-gel synthesis.
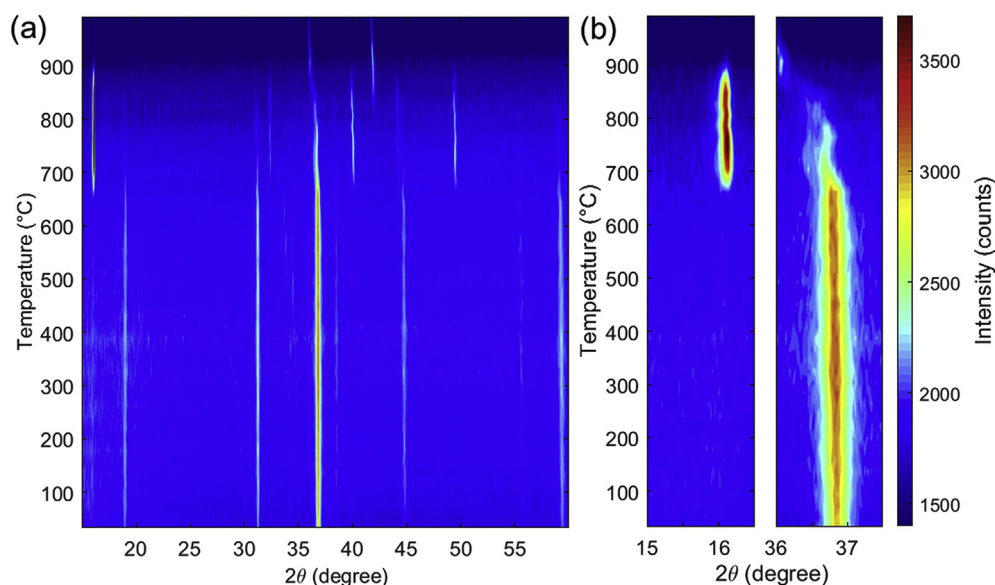

Fig. 2. In situ XRD patterns of Na treated dried precursor sol gel powder collected at various temperatures from room temperature up to 1000 °C, (a) contour plot of in situ XRD patterns, (b) 2θ region of 15–16.5° and 36–37.5° showing the evolution of most intense peak corresponding to reaction during sol-gel synthesis.

transition to NaCo$_2$O$_4$ is less abrupt.

Fig. 3 shows the SEM micrographs and room temperature diffraction patterns of SG powders calcined at different temperatures. The diffraction patterns of the dried sol-gel powder shows a broad peak at 20–25° indicating limited crystallization as would be expected from a sol-gel powder dried at 90 °C. The two strong peaks visible at ~39° and 44° are associated with the aluminium holder on the XRD stage. The diffraction peaks indicate that powder calcined at 450 °C consists of Co$_3$O$_4$ (JCPDS 42-1467) agreeing with results from in-situ studies. The diffraction pattern of powder calcined at 700 °C shows peaks corresponding to those assigned to NaCo$_2$O$_4$ (JCPDS 27-0682) again agreeing with the in-situ data. The powder formed a closed porous structure when dried but on calcining formed a delicate open structure consisting of plate-like

grains consistent with hexagonal NaCo$_2$O$_4$. The use of a relatively low calcination temperature made it possible to maintain a similar level of sodium throughout the synthesis process. The average particle size of the SG powder was found to be less than 1 μm with a degree of particle coarsening during processing at 700 °C. Powder calcined at 700 °C for 6 h gave sufficient purity and suitable grain size for pellet production.

Fig. 4 shows the XRD pattern for NaCo$_2$O$_4$ pellets sintered at 950 °C and 1000 °C. It can be seen that except for the peaks associated with NaCo$_2$O$_4$, in most cases no peaks associated with Co$_3$O$_4$ or other Co oxides were detected, indicating that the NaCo$_2$O$_4$ was stable under these conditions. Higher sintering temperature together with prolonged sintering time resulted in the emergence of an additional peak below 16° (2Θ). A peak in this region is often
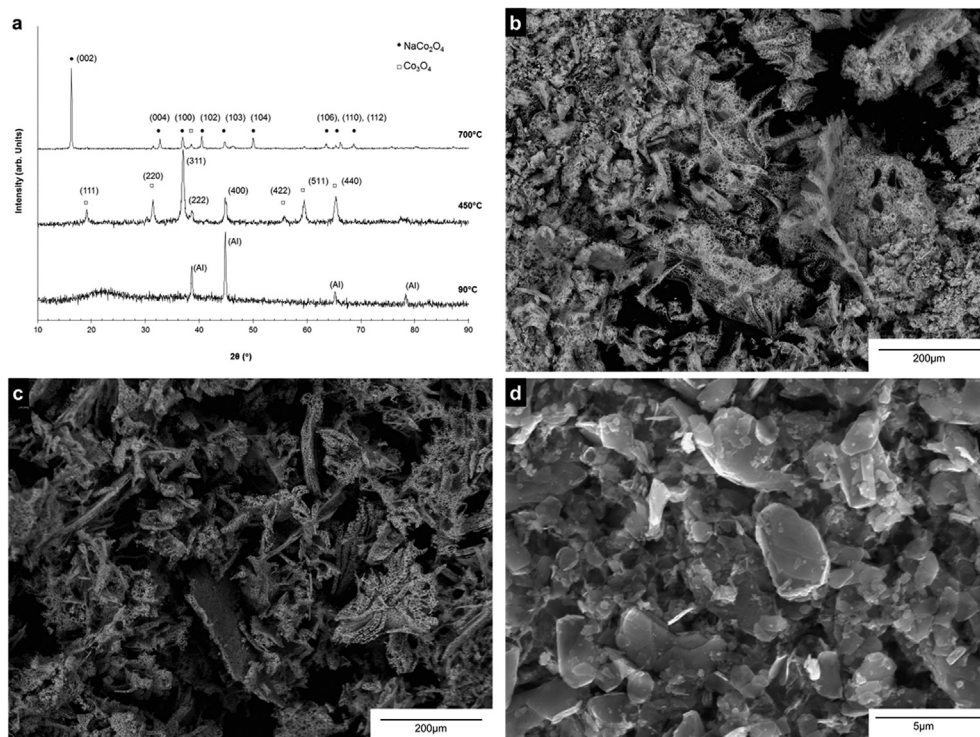
Fig. 3. a) Room temperature XRD patterns of dried sol-gel synthesised powder and powder calcined at 450 °C and 700 °C for 6 h. Presence of characteristic peaks assigned to $NaCo_2O_4$ (no.27 0682) and Co_3O_4 (JCPDS no.421467) are indicated. SEM micrographs of b) as-prepared powder after calcination at 450 °C for 6 h in air, c) & d) as-prepared powder after calcination at 700 °C for 6 h in air.
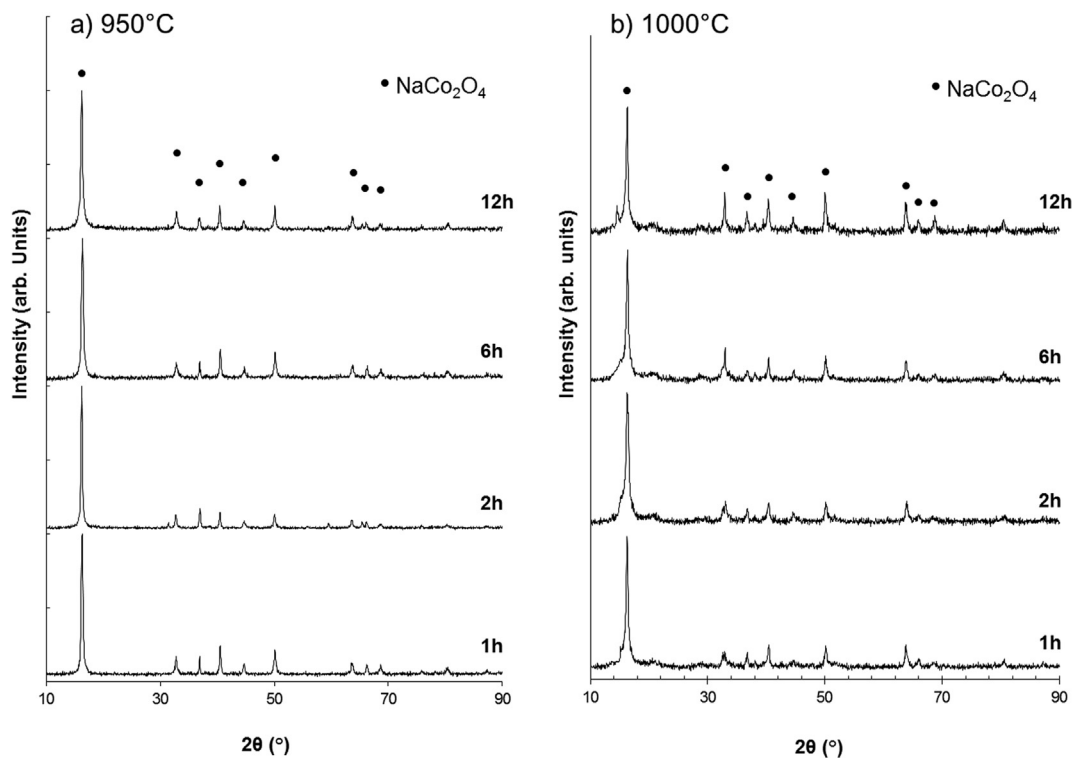

Fig. 4. XRD patterns of $NaCo_2O_4$ sol-gel powder pellets sintered at a) 950 °C and b) 1000 °C for 1, 2, 6 and 12 h, respectively. Presence of characteristic peaks assigned to $NaCo_2O_4$ (JCPDS 27-0682) is indicated. Sintering at 1000 °C leads to a noted degradation of the material and the formation of secondary XRD peaks.

ascribed in literature to the partial hydration or decomposition of samples following storage in air [19,20]. The appearance of peaks at lower angles is often accompanied by a reduction in intensity of peaks corresponding to $NaCo_2O_4$, in particular associated with (002 reflection). In this work, the appearance of the 16° peaks was found primarily for pellets sintered at the higher temperature (1000 °C). This observation suggests that pellets treated at 1000 °C for 12 h are more moisture-sensitive than other samples/conditions.

The microstructure of SG pellets sintered at 950 °C and 1000 °C (Fig. 5) show a fine grained and relatively dense structure over the whole range of sintering times. In both cases the pellets can be seen to exhibit elongation of the grains during sintering, typical of layered crystal structures. However the grain elongation of samples sintered at 1000 °C was more marked than those sintered at 950 °C with increases in both length and width of grains. Samples sintered at 950 °C for up to 6 h had a lateral grain size of 10–15 μm and a grain thickness of 1–2 μm. This increased to 15–20 μm and 2–3 μm on sintering for 12 h. Samples sintered at 1000 °C were composed of significantly bigger grains, being 5–10 μm thick. For sintering times of 1–2 h the grains had lateral dimensions of 20–25 μm, which increased to 25–30 μm when sintered for 6 or 12 h.

Pellets sintered at 900 °C and below exhibited minimal densification as densification requires the diffusion of all atomic species and at such temperatures Co is insufficiently mobile. All samples
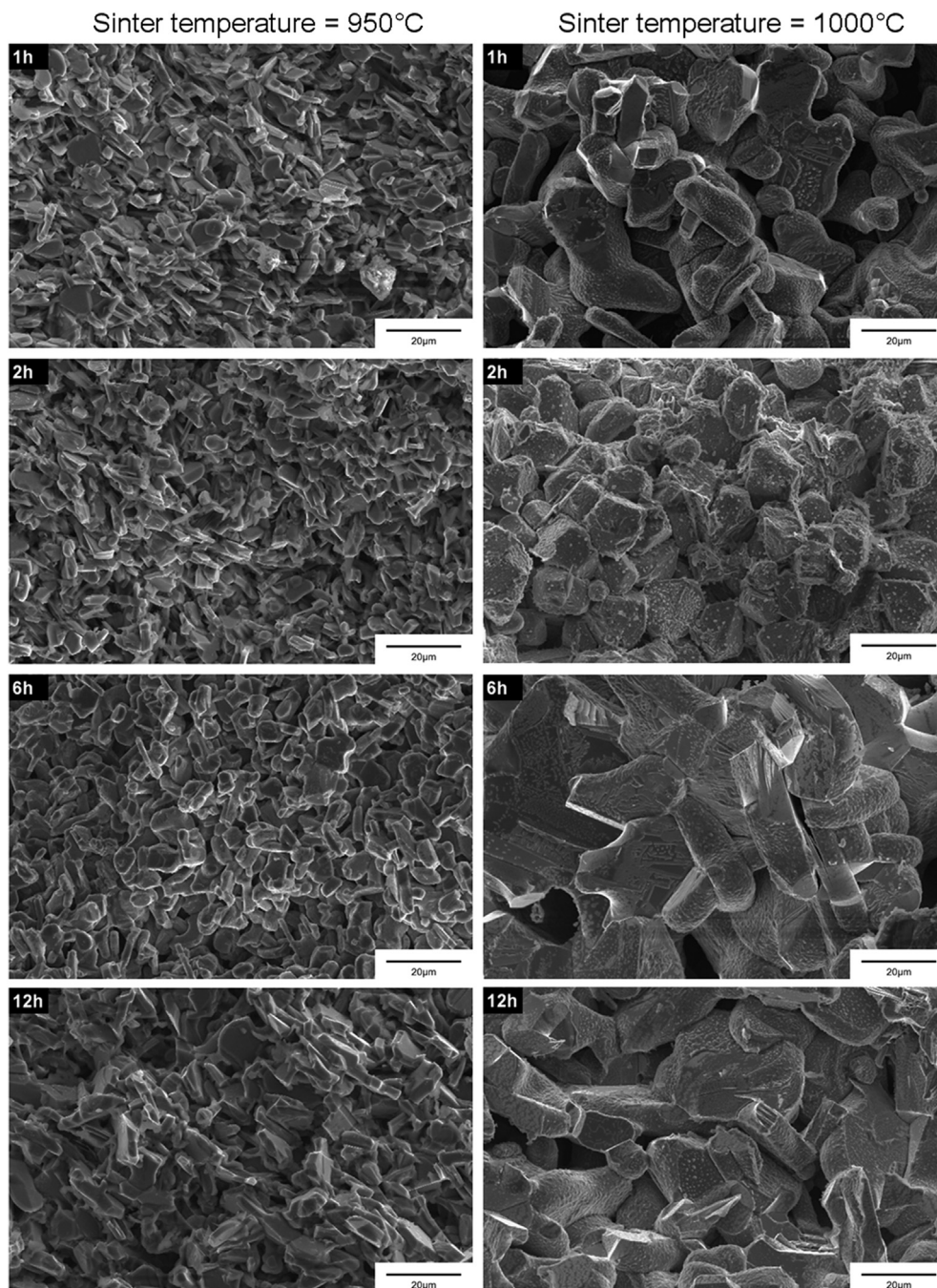

Fig. 5. SEM micrograph of cross sections of pellets prepared from powder synthesised by the sol-gel (SG) method sintered at a) 950 °C and b) 1000 °C. Influence of increasing sintering time results in a significant change in microstructure.

sintered at 950 and 1000 °C for 1 or 2 h exhibited a degree of densification with relative densities of 70 and 80%, respectively. For longer sintering times a difference in density was observed with samples sintered at 950 °C attaining densities of ~85% after 12 h, while samples sintered at 1000 °C had a relative density of 80% due to grain coarsening preventing further densification. The presence of pores has a strong negative effect on both the electrical and thermal conductivity. In a system where only macro-scale porosity is changing the effect on thermoelectric performance should be minimal as both thermal and electrical conductivities would be affected equally.

Fig. 6 shows the XRD pattern for NaCo$_2$O$_4$ sol-gel Na-enriched pellets sintered at 950 °C and 1000 °C. As with the standard SG powder pellets only NaCo$_2$O$_4$ peaks are seen for the majority of samples, with additional peaks emerging again for those sintered at extreme time and temperature. The influence of sintering time on the microstructure for sintering at 950 °C and 1000 °C is shown in Fig. 7. The general behaviour of Na-SG powders was similar to that of SG powder with increasing grain size and density with sintering time. When compared to unmodified sol-gel powder the Na-SG pellets sintered at 950 °C had grains that were 1.5–2 times thicker. A similar behaviour was not observed in the samples sintered at 1000 °C. The addition of Na enhanced densification, leading to final densities of 95% and 90% for samples sintered at 950 and 1000 °C, respectively. With the increase of sintering temperature, further smoothing of the surface can be seen, although these differences are small with increasing sintering time. For pellets sintered at 1000 °C cross sectional micrographs show a distinctly different microstructure.

3.2. Electrical and thermal properties

The results obtained from SG and Na-SG samples sintered under different conditions are presented in Tables 1 and 2, respectively. For samples sintered at 950 °C the lowest values of thermal conductivity were exhibited by pellets sintered for 12 h. In the case of those sintered at 1000 °C SG samples exhibited the lowest conductivity at short sinter times while for Na-SG materials the lowest thermal conductivity was exhibited at high sinter times, potentially indicating the stabilising effect of the Na. In all cases the samples with low thermal conductivity were characterised by a high density and complex grain/microstructure.

The Weidemann-Franz law describes the relationship between electric and thermal conductivity originating from electron transport. In a metal, where thermal conductivity is dominated by electron conduction, this relationship is given by $\kappa = LT\sigma$, where L is the Lorenz number (2.45×10^{-8} WΩK^{-2}). By comparing the electric and thermal conductivities of the materials produced here one can obtain an estimation of the contribution of lattice thermal conductivity (Fig. 8). It can be seen that phonon thermal conductivity plays a significant role (~10× that of electron thermal conductivity) in the material, similar to previous reports [10]. By comparing the data to that of samples produced using solid state synthesis (average powder size >1 μm) and sintered at 950 °C it can be seen that phonon conductivity is reduced when sol-gel derived powder is used. Furthermore, the Na-addition can be seen to further reduce the phonon conducting component due to the refined grain structure and improved scattering centres. For samples sintered at 950 °C prolonged sintering leads to a higher density and a more complex microstructure, typical of the NaCo$_2$O$_4$ layered crystal structure, with grains exhibiting a more pronounced plate-like appearance. The tendency to produce distinct crystallites is enhanced when excess Na is present, as the NaOH is able to act as a flux assisting the required atomic diffusion. The electrical conductivity of all samples exhibits the same dependence on porosity ($\sigma \approx \sigma_0 \exp^{-1.4Vfp}$, where Vfp is the volume fraction of porosity and σ_0 is the conductivity of a fully dense material). It would be expected that thermal conductivity would exhibit the same dependence if the bulk material were unchanged. The reverse behaviour observed here suggests this is not so and that the material structure
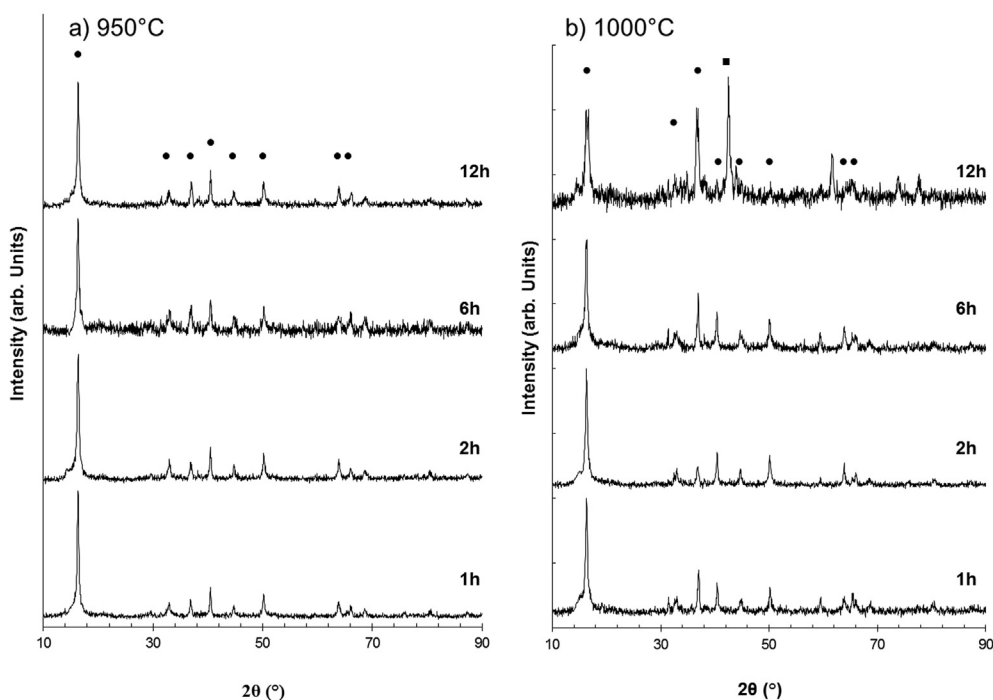

Fig. 6. XRD patterns of Na-enriched NaCo$_2$O$_4$ sol-gel powder pellets sintered at a) 950 °C and b) 1000 °C for 1, 2, 6 and 12 h, respectively. Presence of characteristic peaks assigned to NaCo$_2$O$_4$ (JCPDS 27-0682) is indicated. Sintering at 1000 °C leads to a noted degradation of the material and the formation of secondary XRD peaks.

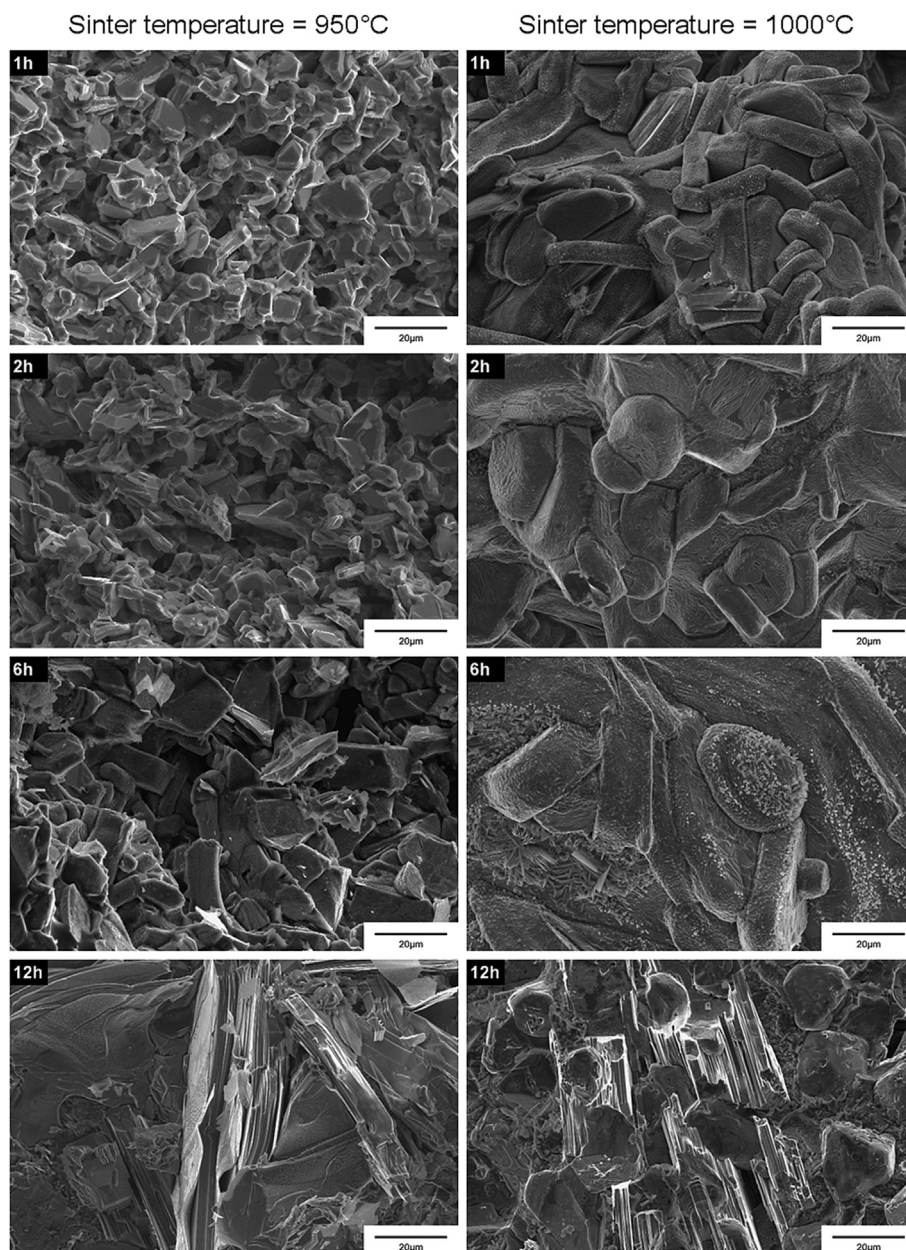Sinter temperature = 950°C   Sinter temperature = 1000°C

Fig. 7. SEM micrograph of cross sections of pellets prepared from Na-enriched powder synthesised by the sol-gel (SG) method sintered at a) 950 °C and b) 1000 °C. Influence of increasing sintering time results in a significant change in microstructure.

Table 1
Near room temperature thermal and electrical properties of sol-gel (SG) samples sintered at 950 °C and 1000 °C for different times.

Sintering temperature		950 °C				1000 °C			
Sintering time		1hr	2hr	6hr	12hr	1hr	2hr	6hr	12hr
Thermal conductivity, κ	Wm^{-1}K^{-1} (±0.1)	1.30	1.18	0.96	0.66	0.60	0.60	0.74	1.20
Electrical conductivity	x10^3 Sm^{-1}	3.2	3.6	3.9	4.0	3.8	3.9	2.6	3.9
Seebeck coefficient	μV/K	30.1	34.1	34.3	34.9	29.8	33.0	34.1	33.4
Power factor	×10^{-6} Wm^{-1}K^{-2}	**2.91**	**4.17**	**4.61**	**4.83**	**3.40**	**4.24**	**3.07**	**4.34**
ZT (@279 K)		**0.0007**	**0.0011**	**0.0014**	**0.0022**	**0.0017**	**0.0021**	**0.0012**	**0.0011**

becomes more complex, with more scattering centres, and is able to counteract the increase in conductivity caused by reduction in porosity. Samples sintered at 1000 °C tended to show an increase in thermal conductivity with sintering time indicating that the complexity of the microstructure is unchanged and only densification and grain growth occur, both of which result in increased

Table 2
Near room temperature thermal and electrical properties of NaOH pre-treated sol-gel (Na-SG) samples sintered at 950 °C and 1000 °C for different times.

Sintering temperature		950 °C				1000 °C			
Sintering time		1hr	2hr	6hr	12hr	1hr	2hr	6hr	12hr
Thermal conductivity, κ	$Wm^{-1}K^{-1}$ (±0.1)	0.92	1.02	0.7	0.7	0.86	0.76	0.92	0.7
Electrical conductivity	$x10^3$ Sm^{-1}	3.5	3.8	4.6	5.0	3.9	4	4.7	3.2
Seebeck coefficient	µV/K	32.9	34.2	32.5	35.1	35.4	34.2	29.2	-[a]
Power factor	$\times 10^{-4}$ $Wm^{-1}K^{-2}$	**3.82**	**4.48**	**4.85**	**6.19**	**4.91**	**4.74**	**4.04**	-
ZT (@279 K)		**0.0012**	**0.0013**	**0.0020**	**0.0026**	**0.0017**	**0.0018**	**0.0013**	-

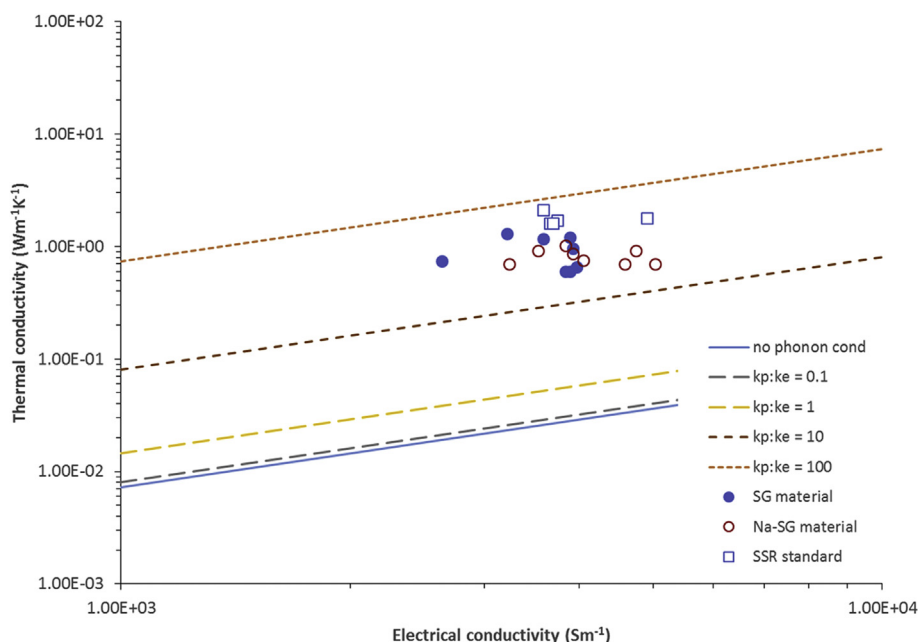[a] Not possible to record a consistent value.

Fig. 8. Relationship of thermal and electrical conductivities (at 297 K) of sodium cobalt oxide pellets produced using Solid State Reaction (SSR), sol-gel synthesised (SG) and Na rich pre-treated sol-gel synthesised (Na-SG) powders at 950 °C and 1000 °C for 1, 2, 6 and 12 h. The solid blue line represents the ideal Weidemann-Franz relationship for materials where thermal conductivity is entirely controlled by electron conduction. Dashed lines show the predicted behaviour for materials where additional phonon conduction occurs alongside electron conduction for cases of κ(phonon):κ(electron) ratios of 0.1, 1, 10 and 100. (For interpretation of the references to colour in this figure legend, the reader is referred to the Web version of this article.)

thermal conductivities. At very high process times/temperatures densification is largely complete and the formation of secondary phase (due to the loss of Na) creates faster phonon conduction paths causing the thermal conductivity to increase again [21]. Where the formation of second phases is disrupted by the addition of extra Na, low thermal conductivity is maintained again showing the intrinsic low thermal conductivity of $NaCo_2O_4$. $NaCo_2O_4$ ceramics with micro-sized grains typically have a room temperature thermal conductivity in the range of $3-5$ $Wm^{-1}K^{-1}$ [22,23] due to a lower amount of grain boundary phonon scattering.

High electrical conductivity is observed for both SG and Na-SG samples sintered at 950 °C for 12 h confirming the positive benefit of high density materials. As these samples also exhibit low thermal conductivity it further strengthens the argument that it is the complex grain structure that is responsible for the reduction in thermal conductivity. For SG samples sintered at 1000 °C there is little variation in electrical conductivity and similar values are observed for Na-SG samples sintered at 1000 °C for 1 and 2 h. A slight increase in conductivity is observed for samples sintered for 6 h but when the time is increased to 12 h the electrical conductivity decreases dramatically, due to loss of Na and formation of an

electrically insulating second phase at the boundaries of grains. Results for samples sintered at 1000 °C indicate that the grain structure is less able to preferentially affect thermal conductivity as would be desirable for thermoelectric applications.

The Seebeck coefficient tends to be highest for samples with good electrical conductivity but there is not a very large variation across all samples which is to be expected as the Seebeck coefficient is independent of porosity. A power factor ($pf = \sigma.\alpha^2$) and dimensionless figure of merit, ZT ($ZT = T.\sigma.\alpha^2/\kappa$) can be calculated. Fig. 9 shows calculated values of ZT and power factor for all samples. Generally the power factor increases with increasing sintering time and temperature. When sintered at 1000 °C both systems exhibit a drop-off in performance at extended sintering times due to the degradation of the structure following loss of Na (Table 1). Values of power factor are broadly consistent with other reports in literature (0.6 [23], 55 [24], 3.1 [25], 2 [26], 0.4 [27], 1.2 [28], 1.4 [29], 5 [30], 18 [31] $\times 10^{-4}$ $Wm^{-1}K^{-2}$). ZT data shows a more pronounced difference between samples due to the bigger changes seen in thermal conductivity. For samples sintered at 950 °C Na pre-treated samples exhibit an enhanced thermoelectric performance relative to untreated sol-gel over the whole range of sintering times. The highest
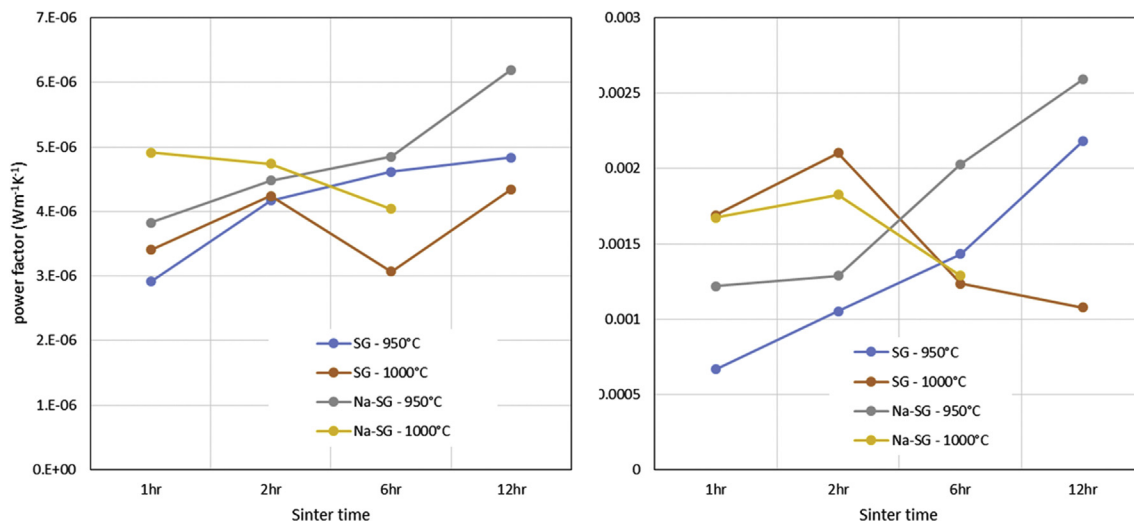
Fig. 9. Power factor and Figure of merit, ZT, of sodium cobalt oxide pellets produced using sol-gel synthesised (SG) and Na rich pre-treated sol-gel synthesised (Na-SG) powders at 950 °C and 1000 °C for 1, 2, 6 and 12 h.

ZT (0.0026) was exhibited by the Na-SG sample sintered at 950 °C for 12 h and was higher than that reported for the untreated samples (maximum 0.0022). The highest ZT is not obtained due to the improvement in a single material property. Instead it is a result of the combined effect of increasing the electrical conductivity and decreasing the thermal conductivity. This is important as it is not a direct effect of improved sintering, caused by the incorporation of extra Na, as this would lead to an increase in both conductivities. This clearly indicates that a more complex microstructure is evolved during sintering that causes increased phonon scattering thereby decreasing thermal conductivity. Fig. 8 highlights the role of adding Na in reducing the proportion of thermal conductivity associated with phonon conduction.

As with the power factor, where the samples were sintered at 1000 °C there is also a dramatic reduction in ZT when sintered for long times clearly highlighting the effect of the loss of volatile Na. Interestingly this is more strongly exhibited in the Na pre-treated sample corresponding to the earlier emergence of secondary peaks in the in situ XRD data. Reports of ZT for $NaCo_2O_4$ materials

are much rarer and typically in the range 0.005—0.05 [23,31] (near to 300 K) which is similar to that obtained for other oxide thermoelectrics at room temperature: e.g. 0.02 for LaSrCoO [32], 0.03 for modified $SrTiO_3$ [33]. The use of small scale sol-gel powders and Na pre-treatments results in $NaCo_2O_4$ samples with higher electrical conductivity and lower thermal conductivity relative to materials produced by standard mixed oxide routes. The Seebeck coefficient is broadly unaltered between the two sol-gel and mixed oxide powders indicating that the grain boundaries (and associated phonon scattering) play a significant role in determining performance of such materials. This may be borne out by studies on films [34], where grains are intrinsically limited in size, which show similar enhanced electrical conductivity. Unfortunately no thermal properties were reported for these films.

The variation in Seebeck coefficient and electrical conductivity as a function of temperature for SG and Na-SG materials is broadly similar. A representative comparison can be seen in the materials sintered at 1000 °C for 6 h shown in Fig. 10. The Seebeck coefficient in both materials increases with temperature in a similar manner.
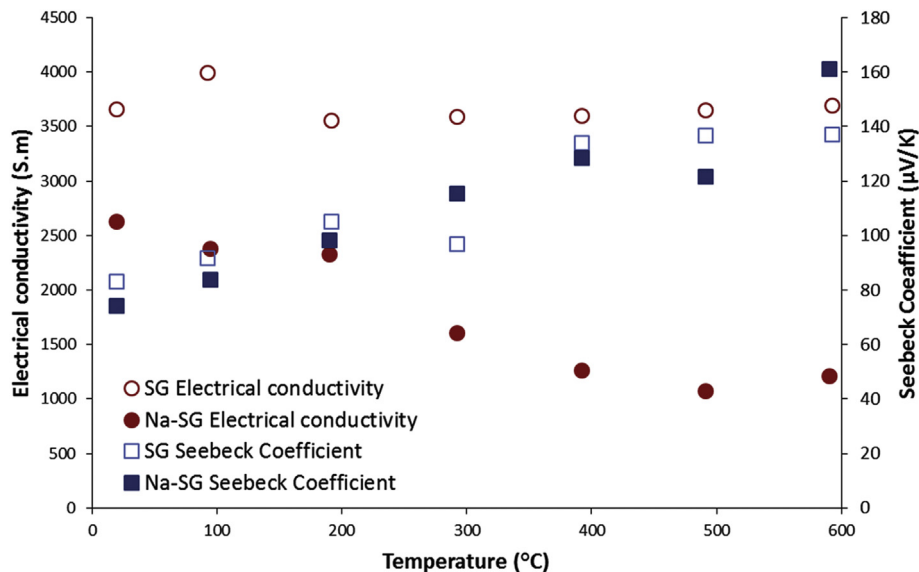

Fig. 10. Electrical conductivity and Seebeck coefficient dependence on temperature for sol-gel synthesised (SG) and Na rich pre-treated sol-gel synthesised (Na-SG) powder sintered 1000 °C for 6 h.

The electrical conductivity shows a slight decrease with increasing temperature which is slightly more pronounced in the Na-SG materials. In both systems the electrical conductivity is approximately constant at temperatures between 400 and 600 °C. This results in an increase in power factor by a factor of 2—3. As thermal conductivity in polycrystalline $NaCo_2O_4$ tends to remain approximately constant with temperature it is reasonable to assume a similar increase in ZT would be observed.

4. Conclusion

In-situ XRD of $NaCo_2O_4$ precursor materials has shown that $NaCo_2O_4$ can be formed at temperatures from around 650 °C, but that the material degrades rapidly at temperatures above 950 °C with a clear degradation of materials observed at temperatures of 1000 °C and above. While $NaCo_2O_4$ forms around 650 °C it does not begin to sinter until at least 900 °C, with 950 °C being required to bring about appreciable densification, resulting in a very small processing window.

Through the pre-treatment of the $NaCo_2O_4$ powder with NaOH, the loss of Na at elevated temperatures can be mitigated. As the addition of NaOH is relatively small, it is unable to compensate for Na loss at high temperatures but at 950 °C it is able to compensate for Na loss and also enhance sintering resulting in improvements in the figure of merit, ZT, of between 20 and 80%. This is due to a combined effect of increased electrical conduction, due to slightly improved densification and mitigating the loss of Na, and decreased thermal conductivity due to enhanced phonon scattering due to the refined complex layered crystal structure. Similar effects are not seen in the samples treated at 1000 °C due to the inability to compensate for the Na loss, and the low thermodynamic stability of $Co_{3-\delta}O_4$ relative to other Co oxide phases. This work has shown that the key to improving ZT in $NaCo_2O_4$ ceramics is a dual approach of encouraging densification and crystal structure refinement while discouraging grain growth. This is challenging in pressureless sintering but it has been shown that the addition of controlled quantities of NaOH can result in material with enhanced performance.

Acknowledgements

References

[1] C. Gayner, K.K. Kar, Recent advances in thermoelectric materials, Prog. Mater. Sci. 83 (2016) 330—382. https://doi.org/10.1016/j.pmatsci.2016.07.002.

[2] C.-H. Kuo, H.-S. Chien, C.-S. Hwang, Y.-W. Chou, M.-S. Jeng, M. Yoshimura, Thermoelectric properties of fine-grained PbTe bulk materials fabricated by cryomilling and spark plasma sintering, Mater. Trans. 52 (4) (2011) 795—801. https://doi.org/10.2320/matertrans.M2010331.

[3] Y. Yin, B. Tudu, A. Tiwari, Recent advances in oxide thermoelectric materials and modules, Vacuum 146 (2017) 356—374. https://doi.org/10.1016/j.vacuum.2017.04.015.

[4] G. Ding, G. Gao, K. Yao, High-efficient thermoelectric materials: the case of orthorhombic IV—VI compounds, Sci. Rep. 5 (2015), 9567. https://doi.org/10.1038/srep09567.

[5] R.A. Dorey, Integrated powder-based thick films for thermoelectric, pyro-electric, and piezoelectric energy harvesting devices, IEEE Sens. J. 14 (7) (2014) 2177—2184. https://doi.org/10.1109/JSEN.2014.2306443.

[6] K. Koumoto, R. Funahashi, E. Guilmeau, Y. Miyazaki, A. Weidenkaff, Y. Wang, C. Wan, Thermoelectric ceramics for energy harvesting, J. Am. Ceram. Soc. 96 (1) (2013) 1—23. https://doi.org/10.1111/jace.12076.

[7] G.-K. Ren, J.-L. Lan, K.J. Ventura, X. Tan, Y.-H. Lin, C.-W. Nan, Contribution of point defects and nano-grains to thermal transport behaviours of oxide-based thermoelectrics, Comput. Mater. 2 (2016), 16023. https://doi.org/10.1038/npjcompumats.2016.23.

[8] Q. Huang, M.L. Foo, J.W. Lynn, H.W. Zandbergen, G. Lawes, Y. Wang, B.H. Toby, A.P. Ramirez, N.P. Ong, R. Cava, Low temperature phase transitions and crystal structure of $Na_{0.5}CoO_2$, J. Phys. Condens. Matter 16 (32) (2004) 5803—5814. https://doi.org/10.1088/0953-8984/16/32/016.

[9] F. Ma, Y. Ou, Y. Yang, Y. Liu, S. Xie, J.-F. Li, G. Cao, R. Proksch, J. Li, Nano-crystalline structure and thermoelectric properties of electrospun NaCo2O4 nanofibres, J. Phys. Chem. C 114 (2010) 22038—22043. https://doi.org/10.1021/jp107488k.

[10] K. Fugita, T. Mochida, K. Nakamura, High-temperature thermoelectric properties of NaxCoO2-δsingle crystals, Jpn. J. Appl. Phys. 40 (2001), 4644-2647, https://doi.org/10.1143/JJAP.40.4644.

[11] M. Takashiri, K. Miyazaki, S. Tanaka, J. Kurosaki, D. Nagai, H. Tsukamoto, Effect of grain size on thermoelectric properties of n-type nanocrystalline bismuth-telluride based thin films, J. Appl. Phys. 104 (8) (2008), 084302. https://doi.org/10.1063/1.2990774.

[12] L.D. Hicks, M.S. Dresselhaus, Thermoelectric figure of merit of a one-dimensional conductor, Phys. Rev. B 47 (24) (1993) 16631—16634. https://doi.org/10.1103/PhysRevB.47.16631.

[13] Z.-H. Chen, G. Han, L. Yang, L. Cheng, J. Zou, Nanostructured thermoelectric materials: current research and future challenge, Prog. Nat. Sci. Mater. Int. 22 (6) (2012) 535—549. https://doi.org/10.1016/j.pnsc.2012.11.011.

[14] L.D. Hicks, T.C. Harman, M.S. Dresselhaus, Use of quantum-well superlattices to obtain a high figure of merit from nonconventional thermoelectric materials, Appl. Phys. Lett. 63 (23) (1993) 3230—3232. https://doi.org/10.1063/1.110207.

[15] S. Maensiri, W. Nuansing, Thermoelectric oxide $NaCo_2O_4$ nanofibers fabricated by electrospinning, Mater. Chem. Phys. 99 (1) (2006) 104—108. https://doi.org/10.1016/j.matchemphys.2005.10.004.

[16] F. Ma, Y. Ou, Y. Yang, Y. Liu, S. Xie, J.-F. Li, G. Cao, R. Proksch, J. Li, Nano-crystalline structure and thermoelectric properties of electrospun $NaCo_2O_4$ nanofibers, J. Phys. Chem. C 114 (50) (2010) 22038—22043. https://doi.org/10.1021/jp107488k.

[17] V.B. Kul'met'eva, S.E. Porozova, B.L. Krasnyi, V.P. Tarasovskii, A.B. Krasnyi, Preparation of zirconia ceramics from powder synthesized by a sol-gel method, Refract. Ind. Ceram. 50 (6) (2009) 438—440. https://doi.org/10.1007/s11148-010-9233-5.

[18] M. Ohtaki, K. Shouji, Strong influence of CO_2 partial pressure on inhomogeneous Na distributions and the thermoelectric performance of polycrystalline $NaCo_2O_4$, in: 24th International Conference on Thermoelectrics ICT 2005, 2005, pp. 472—475. https://doi.org/10.1109/ICT.2005.1519988.

[19] C. Chen, T. Zhang, R. Donelson, D. Chu, R. Tian, T.T. Tan, S. Li, Thermopower and chemical stability of $Na_{0.77}CoO_2/Ca_3Co_4O_9$ composites, Acta Mater. 63 (2014) 99—106. https://doi.org/10.1016/j.actamat.2013.10.011.

[20] C.T. Lin, D.P. Chen, P. Lemmens, X.N. Zhang, A. Maljuk, P.X. Zhang, Study of intercalation/deintercalation of Na_xCoO_2 single crystals, J. Cryst. Growth 275 (3—4) (2005) 606—616. https://doi.org/10.1016/j.jcrysgro.2004.12.021.

[21] A. Benítez-Rico, M.F. García-Sánchez, M. Picquart, B.M. Monroy-Peláez, G. Santana-Rodríguez, Understanding the high ionic conductivity in nano-structured ytterbium stabilized zirconia thin films, J. Nanomater. (2015), 692648. https://doi.org/10.1155/2015/692648.

[22] M.O. Erdal, M. Koyuncu, I. Uslu, The effect of synthesis technique on thermoelectric properties of nanocrystalline $NaCo_2O_4$ ceramics, J. Nanoparticle Res. 16 (2014) 2715. https://doi.org/10.1007/s11051-014-2715-5.

[23] K. Kurosaki, H. Muta, M. Uno, S. Yamanaka, Thermoelectric properties of $NaCo_2O_4$, J. Alloys Compd. 315 (1) (2001), 234-23, https://doi.org/10.1016/S0925-8388(00)01277-9.

[24] I. Terasaki, Transport properties and electronic states of the thermoelectric oxide $NaCo_2O_4$, Physica B 328 (1) (2003) 63—67. https://doi.org/10.1016/S0921-4526(02)01810-0.

[25] J. Chen, Y. Sui, H. Fu, Z. Lu, B. Wei, Z. Qian, J. Miao, Z. Liu, X. Huang, R. Zhu, X. Wang, W. Su, Fabrication and thermoelectric properties of highly textured $NaCo_2O_4$ ceramic, J. Alloys Compd. 407 (1) (2006) 299—303. https://doi.org/10.1016/j.jallcom.2005.06.020.

[26] K. Park, K.U. Jang, H.-C. Kwon, J.-G. Kim, W.-S. Cho, Influence of partial substitution of Cu for Co on the thermoelectric properties of $NaCo_2O_4$, J. Alloys Compd. 419 (1—2) (2006) 213—219. https://doi.org/10.1016/j.jallcom.2005.08.081.

[27] M. Tahashi, M. Takahashi, H. Goto, Thermoelectric performance and crystal phase of calcium cobalt oxides sintered in oxygen gas, J. Am. Ceram. Soc. 101 (2018) 1402—1406. https://doi.org/10.1111/jace.15349.

[28] P. Liu, G. Chen, Y. Cui, H. Zhang, F. Xiao, L. Wang, H. Nakano, High temperature electrical conductivity and thermoelectric power of Na_xCoO_2, Solid State Ionics 179 (39) (2008) 2308–2313. https://doi.org/10.1016/j.ssi.2008.08.010.

[29] Z. Tian, X. Wang, J. Liu, Z. Lin, Y. Hu, Y. Wu, C. Han, Z. Hu, Power factor enhancement induced by Bi and Mn co-substitution in Na_xCoO_2 thermo-electric materials, J. Alloys Compd. 661 (2016) 161–167. https://doi.org/10.1016/j.jallcom.2015.11.084.

[30] H. Yakabe, K. Kikucho, I. Terasaki, Y. Sasago, K. Uchinokura, Thermoelectric properties of transition-metal oxide NaCo2O4 system, XVI ICT '97. Pro-ceedings ICT'97. 16th International Conference on Thermoelectrics, https://doi.org/10.1109/ICT.1997.667584.

[31] E. Ermawan, S. Poertagji, Thermoelectric performance of Na1-xCaxCo2O4, Int. J. Eng. Technol. 15 (2015) 42–45.

[32] O.J. Dura, R. Andujar, M. Falmbigl, P. Rogl, M.A. Lopez de la Torre, E. Bauer, The effect of nanostructure on the thermoelectric figure-of-merit of $La_{0.875}Sr_{0.125}CoO_3$, J. Alloys Compd. 711 (2017) 381–386. https://doi.org/10.1016/j.jallcom.2017.03.335.

[33] D. Srivastava, C. Norman, F. Azough, M.C. Schäfer, E. Guilmeau, R. Freer, Improving the thermoelectric properties of $SrTiO_3$-based ceramics with metallic inclusions, J. Alloys Compd. 731 (2018) 723–730. https://doi.org/10.1016/j.jallcom.2017.10.033.

[34] H.S. Lee, G.H. Kim, D.H. Hwang, S.I. Woo, High thermoelectric power in a Na_xCoO_2 thin film prepared by sputtering with rapid thermal annealing, Curr. Appl. Phys. 15 (3) (2015) 412–416. https://doi.org/10.1016/j.cap.2014.12.030.